ISSN: 2150-4091 Volume 6, Number 16, November 2014

Scientific Research

Natural Science

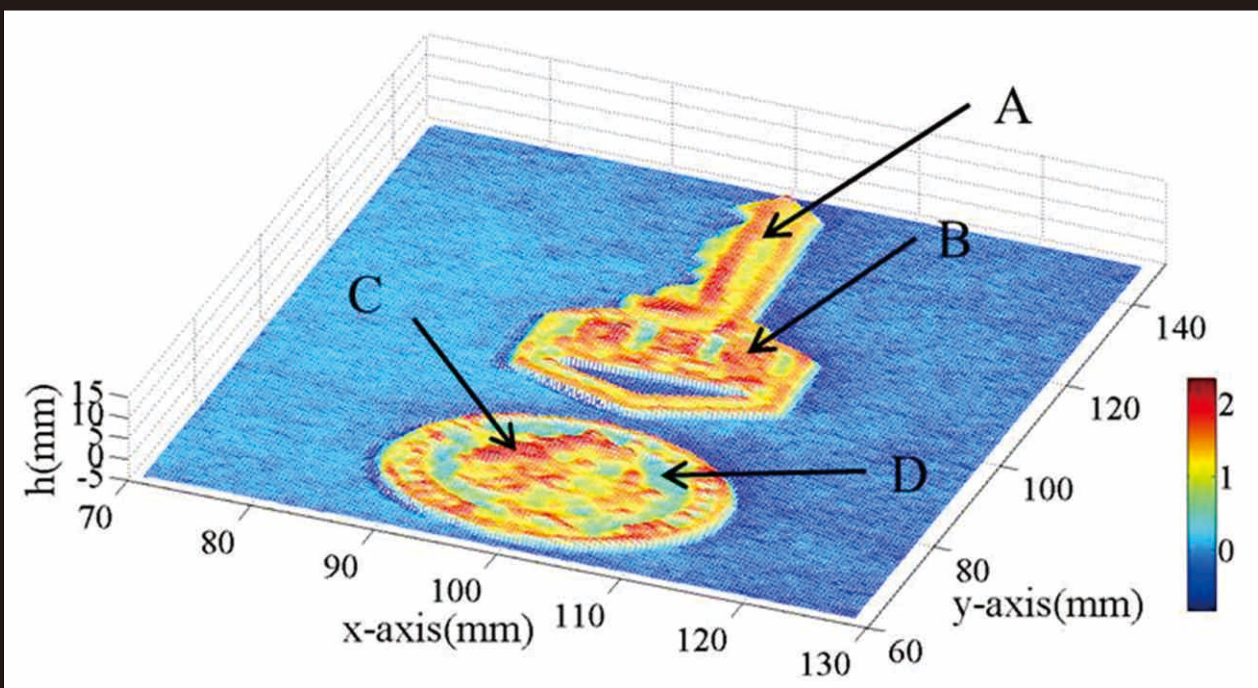

ISSN: 2150-4091
9 772150 409002 16

Editor-in-Chief
Kuo-Chen Chou

www.scirp.org/journal/ns

Journal Editorial Board

ISSN: 2150-4091 (Print) ISSN: 2150-4105 (Online)
http://www.scirp.org/journal/ns

Natural Science, 2014, 6, 1241-1265
Published Online November 2014 in SciRes. http://www.scirp.org/journal/ns

Scientific Research

Table of Contents

Volume 6 Number 16 November 2014

The figure on the front cover is from the article published in Natural Science, 2014, Vol. 6, No. 16, pp. 1253-1258 by Ming-Hung Chiu, Yen-Hsin Chen and Jian-Ming Su.

Natural Science (NS)

Journal Information

SUBSCRIPTIONS

The *Natural Science* (Online at Scientific Research Publishing, www.SciRP.org) is published monthly by Scientific Research Publishing, Inc., USA.

Subscription rates:

Print: $89 per copy.
To subscribe, please contact Journals Subscriptions Department, E-mail: sub@scirp.org

SERVICES

Advertisements
Advertisement Sales Department, E-mail: service@scirp.org

Reprints (minimum quantity 100 copies)
Reprints Co-ordinator,Scientific Research Publishing, Inc., USA.
E-mail:sub@scirp.org

PRODUCTION INFORMATION

For manuscripts that have been accepted for publication, please contact:
E-mail: ns@scirp.org

Natural Science, 2014, 6, 1241-1243
Published Online November 2014 in SciRes. http://www.scirp.org/journal/ns
http://dx.doi.org/10.4236/ns.2014.616112

Capillary Wave's Depth Decay

Kern E. Kenyon

North Lane, Del Mar, California, USA
Email: kernken@aol.com

Received 27 August 2014; revised 20 September 2014; accepted 12 October 2014

Abstract

Depth decay rates for pressure and velocity variations of a propagating capillary wave are found to be significantly different from each other, and neither one is expected to have the classical exponential character. To obtain these results Bernoulli's equation along streamlines in the steady reference frame is combined with the force balance on fluid particles in the cross-stream direction: a pressure gradient offsets the centrifugal force on particles moving along a curved path. The two starting equations for pressure and velocity are nonlinear, but two linear first order ordinary differential equations are produced from them, one for each variable, and they can be integrated immediately. A full solution awaits further information on the non-constant coefficient, the radius of curvature function for the streamlines, either from observations or another theory.

Keywords

Capillary Waves, Depth Decay

1. Introduction

Textbooks of fluid dynamics that mention the capillary wave (or ripples) generally have much less to say about them than they do about the surface gravity wave [1]-[4]. Is this because of their smaller wavelengths and amplitudes? Fundamental properties are not even touched upon, such as the linear and angular momentum of the waves. Presumably, but not stated in the cited references, the fluid particles have an orbital motion, when viewed in the fixed frame, which decays with increasing depth down from the equilibrium free surface. If so, both linear and angular momentum will be propagated with the wave in addition to the better known transport of energy common to all types of waves. Some familiarity with the linear momentum of surface gravity waves comes from its relation to the Stokes drift. From the orbital motion of the fluid particles in propagating waves it is obvious that they possess (orbital) angular momentum.

How the capillary wave motion decays with depth is pretty much taken to be exponential in the classical studies. This is a consequence of assuming irrotational motion with a velocity potential, because when the hori-

How to cite this paper: Kenyon, K.E. (2014) Capillary Wave's Depth Decay. *Natural Science*, **6**, 1241-1243.
http://dx.doi.org/10.4236/ns.2014.616112

zontal motion is selected to be harmonic, *i.e*. wave like, then the vertical motion must be exponential in order to satisfy Laplace's equation for the velocity potential. Physical understanding of the depth decay feature is thereby avoided by this mathematical procedure.

An alternative decay law is proposed below, which in all likelihood will not turn out to be exponential in character. There are advantages and disadvantages to the new approach to describing the capillary wave. A definite advantage is that the governing differential equations for the pressure and velocity, that result from combining two elementary pieces of physics, are linear. Another advantage is that there is no necessity to adopt irrotationality *ab initio*. One disadvantage of the operating equations is that they contain a non-constant coefficient which prevents complete solutions from being obtained at the present time without further theoretical or observational information being supplied to these equations. The non-constant coefficient is the radius of curvature of the streamlines. Measurements will eventually show that the radius of curvature increases with increasing depth from a minimum at the surface to infinity at a depth comparable to a wavelength, and perhaps the exact rate of decay will be uncovered also.

First principle of physics adopted here is the usual law of Bernoulli, where the speed is the greatest, the pressure is the least, applied along streamlines in the steady frame, but with the addition of a novelty: a term involving surface tension of the air/water interface. The second piece is the force balance on fluid particles traveling along curved paths. In the cross-stream direction the centrifugal force is balanced by a pressure gradient. Use of the centrifugal force is not novel but it is still controversial within classical physics.

2. Method

In the steady reference frame the wave shape is motionless to the observer and the fluid flows steadily past him under the wave. Applying Bernoulli's law to the streamline at the air/water interface of the capillary wave yields

$$p = const - \frac{1}{2}\rho U^2 + \frac{T}{R_0} \tag{1}$$

where p is the pressure and U is the fluid speed parallel to the streamline. Constants of the motion on the RHS (right hand side) are $const$ (taken the same for all streamlines), the density ρ and the surface tension T. The radius of curvature at the surface R_0 is computed in the plane of the mean flow.

On the RHS of (1) the third term is not normal. It replaces the usual gravity term, but for capillary waves gravity's influence is assumed to be small compared to that of surface tension. In fact, I have not seen Bernoulli's law displayed anywhere in a text describing capillary waves.

Recently a form of Bernoulli's equation similar to (1) was used to give a qualitative explanation of the *vena contracta*, only there the radius of curvature in the surface tension term is evaluated in the plane perpendicular to the mean flow direction [5].

Consider the vertical distance z to be marked positive upward from the top of a crest where it is zero. Then the balance of forces on a horizontally moving fluid particle at any depth below the crest is

$$\frac{\mathrm{d}p}{\mathrm{d}z} = \frac{\rho U^2}{R} \tag{2}$$

where U, R and p are functions of z. On the LHS (left hand side) of (2) is the pressure force acting down; the centrifugal force acting up is on the RHS. There are now two equations in the two unknowns, ρ, U, and as they stand each of the two equations is nonlinear.

Details of the method will be kept brief because they are similar to those recently produced for the surface gravity wave [6]. Eliminate the velocity between Equations (1) and (2), remembering that below the surface the surface tension term in (1) vanishes since there is no surface tension underneath the air/water interface. The result is a pressure equation

$$\frac{R}{2} \times \frac{\mathrm{d}p}{\mathrm{d}z} + p = const \tag{3}$$

This differential equation is linear, ordinary and of the first order. The non-constant coefficient is R. Solution of (3) begins with the homogeneous part of the equation: the RHS set to zero, followed by separation of variables.

$$\frac{dp}{p} = -\frac{2dz}{R(z)} \tag{4}$$

Both sides of (4) can immediately be integrated to give

$$\ln\left(\frac{p}{p_0}\right) = -2\int\frac{dz}{R} \tag{5}$$

where p_0 is a constant. Then both sides of (5) can be raised to the power of *e* to get

$$\frac{p}{p_0} = e^{-2\int\frac{dz}{R}} \tag{6}$$

Plus an additive constant on the RHS (not displayed). As (6) shows, the depth decay rate for pressure variations is given by the exponent of the exponential on the RHS.

Now, the factor of 2 in the exponent of the RHS of (6) is very significant, as can be made clear. If instead of eliminating the velocity between (1) and (2) to get a pressure equation, the pressure can be eliminated between the same two equations to get the velocity equation by first differentiating (1) with respect to *z*. What will be found is an equation similar to (3) with *U* replacing *p* and with the factor of 2 missing. Then the solution is similar to (6) with *U* replacing *p* and the factor of 2 again missing. Since the depth decay rate for velocity variations equals the exponent in the exponential, which is a factor of 2 smaller than that in (6), this proves that, no matter what $R(z)$ is, pressure variations die away with increasing depth at a faster rate than do the velocity variations. Exactly the same conclusion was found for the surface gravity wave.

Recall the classical result for the surface gravity wave: both pressure and velocity perturbations decrease exponentially with increasing depth down from the equilibrium surface and at the same (*e*-folding) rate. Even though the radius of curvature function $R(z)$ is not exactly known at this point, it is very doubtful that the depth decay rates of the capillary and surface gravity waves will turn out to be the normal exponential one, just from looking at form of Equation (6).

3. Discussion

Finding that the depth rates of decay for pressure and velocity perturbations are significantly different from each other for the capillary wave may come as a surprise to some readers. However, an example of such disparity in steady fluid flow has been available for a few hundred years. Consider a metal cylinder containing water and oriented vertically with gravity acting down. The cylinder has been at constant rotation about its long axis for enough time to establish solid body rotation of the fluid inside it. The horizontal velocity of the flow in the fixed frame of reference is the same as that of the container where they touch and it decreases linearly to zero at the cylinder's center. On the other hand, the air/water interface has a parabolic shape which implies that the water pressure decreases quadratically radially from the rim to the center.

Although not knowing the details of the radius of curvature function for the streamlines may seem bothersome, once it is found, the governing linear equations can be solved immediately, if not analytically then numerically. Also the solutions for pressure and velocity are not sensitive to the exact path, the radius of curvature takes between its minimum values at the surface to infinity at depth because of the integrations involving the curvature on the RHS.

References

[1] Milne-Thomson, L.M. (1953) Theoretical Hydrodynamics. 3rd Edition, MacMillan, New York, 394-397.

[2] Lamb, H. (1945) Hydrodynamics. 6th Edition, Dover, New York, 455-458.

[3] Kundu, P.K. (1990) Fluid Mechanics. Academic Press, San Diego, 205-207.

[4] Faber, T.E. (1995) Fluid Dynamics for Physicists. Cambridge University Press, Cambridge, 173-174. http://dx.doi.org/10.1017/CBO9780511806735

[5] Kenyon, K.E. (2010) Vena Contracta and Surface Tension. *Physics Essays*, **23**, 579. http://dx.doi.org/10.4006/1.3486756

[6] Kenyon, K.E. (2013) Depth Decay Rate of Surface Gravity Wave Pressure and Velocity. *Natural Science*, **5**, 44. http://dx.doi.org/10.4236/ns.2013.51007

Natural Science, 2014, 6, 1244-1252
Published Online November 2014 in SciRes. http://www.scirp.org/journal/ns
http://dx.doi.org/10.4236/ns.2014.616113

Scientific Research

About Lorentz Invariance and Gauge Symmetries: An Alternative Approach to Relativistic Gravitation

Richard Bonneville

Centre National d'Etudes Spatiales (CNES), 2 Place Maurice Quentin, Paris, France
Email: richard.bonneville@cnes.fr

Received 11 September 2014; revised 26 September 2014; accepted 8 October 2014

Abstract

An alternative presentation of a relativistic theory of gravitation, equivalent to general relativity, is given. It is based upon the restriction of the Lorentz invariance of special relativity from a global invariance to a local one. The resulting expressions appear rather simple as we consider the transformations of a local set of pseudo-orthonormal coordinates and not the geometry of a 4-dimension hyper-surface described by a set of curvilinear coordinates. This is the major difference with the usual presentations of general relativity but that difference is purely formal. The usual approach is most adequate for describing the universe on a large scale in astrophysics and cosmology. The approach of this paper, derived from particle physics and focused on local reference frames, underlines the formal similarity between gravitation and the other interactions inasmuch as they are associated to the restriction of gauge symmetries from a global invariance to a local one.

Keywords

Gravitation, General Relativity, Gauge Symmetries

1. Introduction

In the usual presentations of general relativity [1], space-time geometry is described via any set of 4 curvilinear coordinates $\left\{q^{\alpha}\right\}$; an elementary space-time path $\mathrm{d}s$ is expressed as $\mathrm{d}s^2 = -g_{\alpha\beta}\mathrm{d}q^{\alpha}\mathrm{d}q^{\beta}$ where the quadratic form $g_{\alpha\beta}$ characterizes the local metrics. The stake is to express the laws of physics in that frame; for example in the absence of other external forces than gravitation, a particle follows the minimum path $\int_A^B \mathrm{d}s$

How to cite this paper: Bonneville, R. (2014) About Lorentz Invariance and Gauge Symmetries: An Alternative Approach to Relativistic Gravitation. *Natural Science*, **6**, 1244-1252. http://dx.doi.org/10.4236/ns.2014.616113

between two space-time points A and B. In the presence of a gravitation field there is no global transformation of the coordinates allowing the $g_{\alpha\beta}$ to take in the whole space-time the simple form of a Minkowski metrics; nevertheless it can take this special form in a particular point by a suitable change of coordinates which simply consists in diagonalizing $g_{\alpha\beta}$ in this point [2].

We give here an alternative presentation of a relativistic theory of gravitation, equivalent to general relativity, in which gravitation is introduced as a gauge field associated to restricting the global Lorentz invariance of special relativity to a local one.

The presentation of gravitation as a gauge field has been first introduced by Lanczos in the context of a variational approach to general relativity [3] [4]. Then it has been highlighted in an extension of the Yang-Mills approach of particle physics [5]-[7]. In the later, the fundamental interactions are accounted for by the restriction of gauge symmetries from a global invariance to a local one [8]. Those interactions (electro-magnetic, weak, strong) are associated to symmetry groups isomorphic to $\mathrm{U}(1), \mathrm{SU}(2), \mathrm{SU}(3)$, whose elements are unitary transformations [9] [N.B.: by isomorphism between two groups, we mean that their Lie algebras possess the same commutation relations]. When that approach is applied to gravitation, the equivalence principle, central in general relativity [10], is not explicitly assumed but rather derived from the fact that the gauge field is supposed to be minimally coupled.

That restriction from a global invariance to a local one, associated to the emergence of a force field, is indeed a deep similarity between gravitation and the other interactions. However the Lorentz group is isomorphic to the special complex linear group $\mathrm{SL}(2,\mathrm{C})$ whose elements are not unitary and this is an essential difference between gravitation and the other interactions.

In the present work, we assume that the Lorentz group invariance is not a global symmetry of space-time but a local symmetry of a 4-dimension hyper-surface, which can be thought of as embedded in a space with a larger number of dimensions and we consider the transformations of a local set of pseudo-orthonormal coordinates and not the geometry of the 4-dimension hyper-surface described by a set of curvilinear coordinates. This is a major difference with other presentations of relativistic gravitation; its interest is to lead to facially simpler expressions although that difference is essentially formal.

2. Gauge Properties

Let us consider the 4-dimension space-time of special relativity and a pseudo-orthonormal base $\{\mathbf{e}_0, \mathbf{e}_1, \mathbf{e}_2, \mathbf{e}_3\}$ with the Minkowski metrics

$$\boldsymbol{\eta}_{\mu\nu} = \begin{pmatrix} -1 & 0 & 0 & 0 \\ 0 & 1 & 0 & 0 \\ 0 & 0 & 1 & 0 \\ 0 & 0 & 0 & 1 \end{pmatrix} \tag{1}$$

Any infinitesimal transformation $\mathbf{R}$ of the Lorentz group can be written as

$$\mathbf{R} = \mathbf{I} + \begin{pmatrix} 0 & -\beta_x & -\beta_y & -\beta_z \\ -\beta_x & 0 & \alpha_z & -\alpha_y \\ -\beta_y & -\alpha_z & 0 & \alpha_x \\ -\beta_z & \alpha_y & -\alpha_x & 0 \end{pmatrix} \tag{2}$$

$\mathbf{R}$ conserves the pseudo norm $-x_0^2 + x_1^2 + x_2^2 + x_3^2 = -c^2t^2 + x^2 + y^2 + z^2$. It can alternatively be written as

$$\mathbf{R} = \mathbf{I} + i\vec{\alpha} \cdot \vec{\mathbf{J}} + i\vec{\beta} \cdot \vec{\mathbf{K}} \tag{3}$$

where $\vec{\alpha}$ et $\vec{\beta}$ are 2 vectors of the ordinary 3-dimension-space. $\mathbf{J}_x, \mathbf{J}_y, \mathbf{J}_z, \mathbf{K}_x, \mathbf{K}_y, \mathbf{K}_z$ are the 6 infinitesimal generators of the Lorentz group $\Lambda(4)$, the $\mathbf{J}_p$ s are hermitic $\left(\mathbf{J}_p^\dagger = \mathbf{J}_p\right)$, whereas the $\mathbf{K}_p$ s are antihermitic $\left(\mathbf{K}_p^\dagger = -\mathbf{K}_p\right)$, the pseudo vector $\vec{\mathbf{J}}$ and the true vector $\vec{\mathbf{K}}$ respectively account for rotations and for Lorentz transformations; α_z stands for a rotation angle around the Z axis, and β_z for the velocity of a Lorentz transformation along the Z axis.

We introduce the 2 anti-symmetric tensors

$$\mathbf{L}^{\rho\sigma} = \begin{pmatrix} \mathbf{0} & \mathbf{K}_x & \mathbf{K}_y & \mathbf{K}_z \\ -\mathbf{K}_x & \mathbf{0} & \mathbf{J}_z & -\mathbf{J}_y \\ -\mathbf{K}_y & -\mathbf{J}_z & \mathbf{0} & \mathbf{J}_x \\ -\mathbf{K}_z & \mathbf{J}_y & -\mathbf{J}_x & \mathbf{0} \end{pmatrix} \tag{4}$$

and

$$\mathbf{\Omega}_{\rho\sigma} = \begin{pmatrix} 0 & \beta_x & \beta_y & \beta_z \\ -\beta_x & 0 & \alpha_z & -\alpha_y \\ -\beta_y & -\alpha_z & 0 & \alpha_x \\ -\beta_z & \alpha_y & -\alpha_x & 0 \end{pmatrix} \tag{5}$$

Each component $\mathbf{J}_p$ or $\mathbf{K}_p$ is a 4 × 4 matrix so that $\mathbf{R}$ can be written as

$$\mathbf{R} = \mathbf{I} + \frac{i}{2}\underline{\underline{\mathbf{\Omega}}} : \underline{\underline{\mathbf{L}}} = \mathbf{I} + \frac{i}{2}\mathbf{\Omega}_{\rho\sigma}\mathbf{L}^{\rho\sigma} \tag{6}$$

More generally, any transformation of the Lorentz group can be figured by

$$\mathbf{R}(\mathbf{\Omega}) = \exp\frac{i}{2}\underline{\underline{\mathbf{\Omega}}} : \underline{\underline{\mathbf{L}}} \tag{7}$$

We now assume that the Lorentz group invariance is not a global symmetry of space-time but a local symmetry of a 4-dimension hyper-surface, which can be thought of as embedded in a space with a larger number of dimensions, for example 10 as it is envisaged in many unification theories. If we consider the tangent plane to this hyper-surface in any point *M*, it is possible to define in this plane a pseudo-orthonormal reference frame, and in fact an infinite set of similar frames deduced from each other by a Lorentz transformation or a rotation; in the close vicinity of M the laws of physics are invariant under the Lorentz group. We can in another point M' of the hyper-surface M' define a similar set of pseudo-orthonormal frames. The question is: what is the correspondence between the 2 sets of reference frames attached to *M* and M'?

Let us first perform on the surface an infinitesimal displacement $\mathbf{T}(\boldsymbol{\varepsilon})$ from *M* to $M' = M + \mathrm{d}M$; in this close vicinity of *M* the surface is assimilated to its tangent plane and $\mathbf{T}(\boldsymbol{\varepsilon})$ is an infinitesimal translation. Then we perform a transformation $\mathbf{R}(\mathbf{\Omega})$ around M'. If $\mathbf{\Omega}$ is a constant, the coordinates of M' are

$$x'^{\mu} = \left[\exp\frac{i}{2}\underline{\underline{\mathbf{\Omega}}} : \underline{\underline{\mathbf{L}}}\right]^{\mu}_{\nu}\left(x^{\nu} + \varepsilon^{\nu}\right) = \left[\exp\frac{i}{2}\underline{\underline{\mathbf{\Omega}}} : \underline{\underline{\mathbf{L}}}\right]^{\mu}_{\nu} x^{\nu} + \left[\exp\frac{i}{2}\underline{\underline{\mathbf{\Omega}}} : \underline{\underline{\mathbf{L}}}\right]^{\mu}_{\nu} \varepsilon^{\nu} \tag{8}$$

But if $\mathbf{\Omega}$ is a function of the point *M*, that expression becomes:

$$\begin{aligned} x'^{\mu} &= \left[\exp\frac{i}{2}\underline{\underline{\mathbf{\Omega}}}(M + \mathrm{d}M) : \underline{\underline{\mathbf{L}}}\right]^{\mu}_{\nu}\left(x^{\nu} + \varepsilon^{\nu}\right) \\ &= \left[\exp\frac{i}{2}\underline{\underline{\mathbf{\Omega}}}(M) : \underline{\underline{\mathbf{L}}}\right]^{\mu}_{\nu} x^{\nu} + \left[\exp\frac{i}{2}\underline{\underline{\mathbf{\Omega}}} : \underline{\underline{\mathbf{L}}}\right]^{\mu}_{\nu} \varepsilon^{\nu} + \frac{i}{2}\left[\exp\frac{i}{2}\underline{\underline{\mathbf{\Omega}}} : \underline{\underline{\mathbf{L}}}\right]\left[\varepsilon^{\rho}\partial_{\rho}\underline{\underline{\mathbf{\Omega}}} : \underline{\underline{\mathbf{L}}}\right]^{\mu}_{\nu} x^{\nu} \end{aligned} \tag{9}$$

Comparing the two expressions Equation (8) and Equation (9) above, we see that ε^{μ} is transformed into

$$\varepsilon^{\mu} + \varepsilon^{\nu}\mathbf{G}^{\mu}_{\nu} \tag{10}$$

with

$$\mathbf{G}^{\mu}_{\nu} = \frac{i}{2}\left[\partial_{\nu}\underline{\underline{\mathbf{\Omega}}} : \underline{\underline{\mathbf{L}}}\right]^{\mu}_{\rho} x^{\rho} \tag{11}$$

Now considering some function $\mathbf{\Phi}(M)$, we deduce that

$$\mathbf{\Phi}(M + \mathrm{d}M) = \mathbf{\Phi}\left(x^{\mu}\right) + \varepsilon^{\mu}\partial_{\mu}\mathbf{\Phi} \tag{12}$$

is in a similar way transformed into

$$\mathbf{\Phi}\left(x^{\mu}\right)+\varepsilon^{\mu}\partial_{\mu}\mathbf{\Phi}+\varepsilon^{\nu}\mathbf{G}_{\nu}^{\mu}\partial_{\mu}\mathbf{\Phi} \tag{13}$$

i.e. ∂_{μ} is replaced by

$$D_{\mu}=\partial_{\mu}+\mathbf{G}_{\mu}^{\nu}\partial_{\nu} \tag{14}$$

The impulsion

$$\mathbf{p}^{\mu}=i^{-1}\partial^{\mu}=i^{-1}\mathbf{\eta}^{\mu\nu}\partial_{\nu}=\left(i\frac{\partial}{\partial t},\ i^{-1}\vec{\nabla}\right) \tag{15}$$

is the infinitesimal generator of space-time translations. Equation (14) above means that $\mathbf{p}^{\mu}$ is replaced by

$$\mathbf{P}^{\mu}=i^{-1}D^{\mu}=\mathbf{p}^{\mu}+G_{\lambda}^{\mu}\mathbf{p}^{\lambda} \tag{16}$$

The orbital angular momentum anti-symmetric tensor

$$\mathbf{l}^{\rho\sigma}=\mathbf{x}^{\rho}\mathbf{p}^{\sigma}-\mathbf{x}^{\sigma}\mathbf{p}^{\rho}=i^{-1}\left(x^{\rho}\partial^{\sigma}-x^{\sigma}\partial^{\rho}\right) \tag{17}$$

can be written as

$$\mathbf{l}^{\rho\sigma}=i^{-1}\,\partial/\partial\varphi_{\rho\sigma} \tag{18}$$

where $\varphi_{\rho\sigma}$ denotes a rotation angle in the $(\rho\sigma)$ plan (N.B.: the 3-dimension vector components $\mathbf{j}_{p}=\varepsilon_{pqr}\mathbf{l}^{qr}$ and $\mathbf{k}_{p}=\mathbf{l}^{0p}$ also satisfy the commutation relations above). Since $\mathbf{\Omega}_{\rho\sigma}=-\mathbf{\Omega}_{\sigma\rho}$, then

$$D_{\mu}=\partial_{\mu}+\frac{i}{2}x^{\rho}\left[\partial_{\mu}\underline{\underline{\mathbf{\Omega}}}:\underline{\underline{\mathbf{L}}}\right]_{\rho}^{\nu}\partial_{\nu} \tag{19a}$$

can be written as

$$D_{\mu}=\partial_{\mu}+\frac{i}{4}\mathbf{\eta}_{\mu\sigma}\left[\frac{\partial\underline{\underline{\mathbf{\Omega}}}}{\partial\varphi_{\rho\sigma}}:\underline{\underline{\mathbf{L}}}\right]_{\rho}^{\nu}\partial_{\nu} \tag{19b}$$

That expression allows to evidence a gauge invariance property: it is possible to add to $\mathbf{\Omega}_{\rho\sigma}$ any function $\mathbf{\omega}\left(\mathbf{\eta}_{\mu\nu}x^{\mu}x^{\nu}\right)$ without changing $\mathbf{G}_{\nu}^{\mu}$: if $\mathbf{\omega}$ only depends on the invariant quantity $\mathbf{\eta}_{\mu\nu}x^{\mu}x^{\nu}$, its derivation with respect to $\varphi_{\rho\sigma}$ is just 0. As a consequence, there is some flexibility in the determination of the $\mathbf{G}_{\nu}^{\mu}$s and we can impose the 4 gauge conditions

$$\partial_{\mu}\mathbf{G}_{\nu}^{\mu}=0 \tag{20}$$

We have here above considered the transformations of a local set of pseudo-orthonormal coordinates and not the geometry of the 4-dimension hyper-surface described by a set of curvilinear coordinates. This is the major difference with other presentations of relativistic gravitation and notably with general relativity but that difference is purely formal. As a consequence, many mathematical expressions look simpler; for example, the invariant 4-dimension volume element $\mathrm{d}V$ that appears in the expression of the action integral $S=\int\mathcal{L}\mathrm{d}V$ in the Lagrange formalism is merely $\mathrm{d}^{4}\mathbf{x}$, *i.e.* the determinant of the metric tensor is 1.

3. Gravitation Field Equations

We now consider a scalar particle of mass *m* (but the procedure can be straightforwardly generalized to a particle of any spin, be it massive or not) and the Lagrangian density

$$\mathcal{L}=\mathbf{\eta}^{\mu\nu}\dot{\mathbf{\Psi}}_{\mu}^{\dagger}\dot{\mathbf{\Psi}}_{\nu}+\left(mc/\hbar\right)^{2}\mathbf{\Psi}^{\dagger}\mathbf{\Psi} \tag{21a}$$

with

$$\dot{\mathbf{\Psi}}_{\mu}=\partial_{\mu}\mathbf{\Psi} \tag{21b}$$

We perform the transformation $\partial_{\mu}\to D_{\mu}=\partial_{\mu}+\mathbf{G}_{\mu}^{\nu}\partial_{\nu}$ so that the Lagrangian density becomes

$$\mathcal{L} = \mathfrak{g}^{\mu\nu}\dot{\boldsymbol{\Psi}}_\mu^\dagger\dot{\boldsymbol{\Psi}}_\nu + \left(mc/\hbar\right)^2 \boldsymbol{\Psi}^\dagger\boldsymbol{\Psi} \tag{22}$$

where we have introduced the effective metrics

$$\mathfrak{g}_{\mu\nu} = \boldsymbol{\eta}_{\mu\nu} + \mathfrak{h}_{\mu\nu} \tag{23a}$$

with

$$\mathfrak{h}_{\mu\nu} = \boldsymbol{\eta}_{\rho\sigma}\mathbf{G}_\mu^\rho\mathbf{G}_\nu^\sigma + \boldsymbol{\eta}_{\mu\rho}\mathbf{G}_\nu^\rho + \boldsymbol{\eta}_{\nu\sigma}\mathbf{G}_\mu^\sigma \tag{23b}$$

We have written $\mathfrak{g}_{\mu\nu}$ and $\mathfrak{h}_{\mu\nu}$ with gothic letters instead of the usual $\mathbf{g}_{\mu\nu}$ and $\mathbf{h}_{\mu\nu}$ in order to remind ourselves that we have considered a local set of pseudo Cartesian coordinates and not a set of curvilinear coordinates running over the whole surface.

Applying the Lagrange equations to the $\boldsymbol{\Psi}$ field, *i.e.*

$$\partial_\mu \frac{\partial\mathcal{L}}{\partial\dot{\boldsymbol{\Psi}}_\mu} = \frac{\partial\mathcal{L}}{\partial\boldsymbol{\Psi}} \tag{24}$$

gives

$$\left[\mathfrak{g}^{\mu\nu}\partial_\mu\partial_\nu - \left(mc/\hbar\right)^2\right]\Psi + \left(\partial_\mu\mathfrak{g}^{\mu\nu}\right)\left(\partial_\nu\Psi\right) = 0 \tag{25}$$

From the expression of $\mathfrak{g}^{\mu\nu}$ as a function of the $\mathbf{G}_{\mu\nu}$ s it is clear that $\mathfrak{g}^{\mu\nu} = \mathfrak{g}^{\nu\mu}$; $\mathfrak{g}$ has thus 10 components but from the gauge conditions $\partial_\mu\mathbf{G}_\nu^\mu = 0$ we derive

$$\partial_\mu\mathfrak{g}^{\mu\nu} = 0 \tag{26}$$

Equation (26) shows that actually $\mathfrak{g}$ has only 6 independent components. The cross-term in Equation (25) vanishes, leading to

$$\left(\mathfrak{g}^{\mu\nu}\partial_\mu\partial_\nu\right)\boldsymbol{\Psi} - \left(mc/\hbar\right)^2 \boldsymbol{\Psi} = 0 \tag{27}$$

The wave equation so appears as the wave equation of a free particle in which the original Minkowski metrics $\boldsymbol{\eta}_{\mu\nu}$ has been replaced by the effective metrics $\mathfrak{g}_{\mu\nu}$.

The gravitation field is thus described by a modification of the geometry of space-time by replacing the Minkowski metrics $\boldsymbol{\eta}_{\mu\nu}$ by the effective metrics $\mathfrak{g}_{\mu\nu}$. A consequence of the modified wave equation above is that the dynamics of any particle, with or without mass, is affected by a gravitation field.

We now assume for the gravitation field itself a Lagrangian density term quadratic in $\mathfrak{g}$ and in $\partial_\mu\mathfrak{g}$. The scalar product of two vectors $\mathbf{A}$ and $\mathbf{B}$ is $\mathfrak{g}_{\mu\nu}A^\mu B^\nu = A_\mu B^\mu = A^\mu B_\mu$, this can be extended to the scalar product of two tensors of any rank and to the metric tensor itself. So for the term quadratic in $\mathfrak{g}$ we assume the expression

$$\lambda^2\mathfrak{g}_{\alpha\rho}\mathfrak{g}_{\beta\sigma}\mathfrak{g}^{\rho\sigma}\mathfrak{g}^{\alpha\beta} = \lambda^2\mathfrak{g}_\sigma^\alpha\mathfrak{g}_\alpha^\sigma = \lambda^2\mathfrak{g}^{\alpha\beta}\mathfrak{g}_{\alpha\beta} \tag{28}$$

λ is the mass of the gravitation field; now $\mathfrak{g}^{\alpha\beta}\mathfrak{g}_{\alpha\beta} = \mathbf{I}$ so that this term is a constant we can hereunder discard (in fact we will see later on that formally maintaining that term in the calculation would imply $\lambda = 0$). In a similar way we assume for the term quadratic in $\partial_\mu\mathfrak{g}$ the following expression

$$\mathfrak{g}^{\mu\nu}\left(\mathfrak{g}_{\alpha\rho}\partial_\mu\mathfrak{g}^{\rho\beta}\right)\left(\mathfrak{g}_{\beta\sigma}\partial_\nu\mathfrak{g}^{\sigma\alpha}\right) \tag{29a}$$

or

$$\left(\partial^\nu\mathfrak{g}_{\rho\sigma}\right)\left(\partial_\nu\mathfrak{g}^{\rho\sigma}\right) \tag{29b}$$

[N.B.: as $\mathfrak{g}^{\mu\nu}\mathfrak{g}_{\mu\nu}^{\mu\nu} = \mathbf{I}$, considering the infinitesimal variations $\mathfrak{g}^{\mu\nu} \to \mathfrak{g}^{\mu\nu} + \boldsymbol{\delta}^{\mu\nu}$ and $\mathfrak{g}_{\mu\nu} \to \mathfrak{g}_{\mu\nu} + \boldsymbol{\delta}_{\mu\nu}$, and neglecting the second order terms gives $\boldsymbol{\delta}^{\mu\nu} = -\boldsymbol{\delta}_{\mu\nu}$; it then may be checked that the additional terms that could appear in developing the derivatives of Equation (29b) actually cancel each other].

The full Lagrangian density of the (field + particle) system is

$$\mathcal{L} = \left[\mathfrak{g}^{\mu\nu}\partial_\mu\boldsymbol{\Psi}^\dagger\partial_\nu\boldsymbol{\Psi} + \left(mc/\hbar\right)^2 \boldsymbol{\Psi}^\dagger\boldsymbol{\Psi}\right] - \chi^{-1}\mathfrak{g}^{\mu\nu}\left(\mathfrak{g}_{\alpha\rho}\partial_\mu\mathfrak{g}^{\rho\beta}\right)\left(\mathfrak{g}_{\beta\sigma}\partial_\nu\mathfrak{g}^{\sigma\alpha}\right) \tag{30}$$

where χ is a dimensionless constant; the negative sign and the negative exponent are for commodity reasons.

Applying the Lagrange equations to $\mathfrak{g}^{\mu\nu}$, *i.e.*

$$\partial_\xi \frac{\partial \mathcal{L}}{\partial \dot{\mathfrak{g}}^{\mu\nu}} = \frac{\partial \mathcal{L}}{\partial \mathfrak{g}^{\mu\nu}} \tag{31}$$

with $\dot{\mathfrak{g}}^{\mu\nu} = \partial_\xi \mathfrak{g}^{\mu\nu}$ leads to the field equations (with the same remarks as in the N.B. here above):

$$\mathfrak{g}_{\mu\alpha}\mathfrak{g}_{\nu\beta}\left(\mathfrak{g}^{\rho\sigma}\partial_\rho\partial_\sigma\mathfrak{g}^{\alpha\beta}\right) = -\chi\left(\partial_\mu \mathbf{\Psi}\right)^\dagger\left(\partial_\nu \mathbf{\Psi}\right) \tag{32}$$

These are the equations of the gravitation field and their nonlinear character is obvious. The term on the right-hand side

$$\chi\left(\partial_\mu \mathbf{\Psi}\right)^\dagger\left(\partial_\nu \mathbf{\Psi}\right) \tag{33}$$

is proportional to the energy-impulsion density tensor of the particle; it is the source term of the gravitation field. In the classical, *i.e.* non quantum, limit, the correspondence $\mathbf{p}_\mu \leftrightarrow i^{-1}\hbar\boldsymbol{\eta}_\mu^\nu\partial_\nu$ together with the expression of the density $\rho = m\mathbf{\Psi}^\dagger\mathbf{\Psi}$, changes this term into

$$\chi\frac{\rho}{m\hbar^2}\mathbf{p}_\mu\mathbf{p}_\nu = \chi\frac{\rho}{m\hbar^2}\mathbf{T}_{\mu\nu} \tag{34}$$

So Equation (32) becomes

$$\mathfrak{g}^{\mu\nu}\mathfrak{g}_{\mu\alpha}\mathfrak{g}_{\nu\beta}\left(\mathfrak{g}^{\rho\sigma}\partial_\rho\partial_\sigma\mathfrak{g}^{\alpha\beta}\right) = -\chi\frac{\rho}{m\hbar^2}\mathfrak{g}^{\mu\nu}\mathbf{T}_{\mu\nu} \tag{35}$$

For the sake of commodity, we will re-write it in a different, more workable way. Let us introduce the two quantities

$$\mathrm{T} = \mathfrak{g}^{\mu\nu}\mathbf{T}_{\mu\nu} \tag{36a}$$

$$\boldsymbol{\tau}_{\mu\nu} = \mathbf{T}_{\mu\nu} - \frac{1}{2}\mathfrak{g}_{\mu\nu}\mathrm{T} \tag{36b}$$

Combining Equations (35) and (36) we finally get after some manipulations

$$\left(2\mathfrak{g}_{\mu\alpha}\mathfrak{g}_{\nu\beta} - \mathfrak{g}_{\mu\nu}\mathfrak{g}_{\alpha\beta}\right)\left(\mathfrak{g}^{\rho\sigma}\partial_\rho\partial_\sigma\mathfrak{g}^{\alpha\beta}\right) = -2\chi\frac{\rho}{m\hbar^2}\boldsymbol{\tau}_{\mu\nu} \tag{37}$$

4. Non Relativistic Limit

In the case of a weak gravitation field, the quadratic terms in the field equations can be neglected. In the absence of matter, the linearized equations take the form of propagation like equations:

$$\boldsymbol{\eta}^{\mu\nu}\partial_\mu\partial_\nu\mathfrak{h}_{\mu\nu} \approx 0 \tag{38}$$

If matter is present, there is a source term:

$$\left(2\boldsymbol{\eta}_{\mu\alpha}\boldsymbol{\eta}_{\nu\beta} - \boldsymbol{\eta}_{\mu\nu}\boldsymbol{\eta}_{\alpha\beta}\right)\left(\boldsymbol{\eta}^{\rho\sigma}\partial_\rho\partial_\sigma\mathfrak{h}^{\alpha\beta}\right) \approx -2\chi\frac{\rho}{m\hbar^2}\left(\mathbf{T}_{\mu\nu} - \frac{1}{2}\boldsymbol{\eta}_{\mu\nu}\mathrm{T}\right) \tag{39a}$$

with

$$\mathrm{T} \approx \boldsymbol{\eta}^{\rho\sigma}\mathbf{T}_{\rho\sigma} \tag{39b}$$

i.e.

$$\Box\mathfrak{h}_{00} \approx -2\chi\frac{\rho}{m\hbar^2}\left(\mathbf{T}_{00} + \frac{\mathrm{T}}{2}\right) \tag{40a}$$

$$\Box\mathfrak{h}_{ii} \approx -2\chi\frac{\rho}{m\hbar^2}\left(\mathbf{T}_{ii} - \frac{\mathrm{T}}{2}\right) \tag{40b}$$

$$\square\mathfrak{h}_{i0} \approx +\chi\frac{\rho}{m\hbar^2}\mathbf{T}_{i0} \tag{40c}$$

$$\square\mathfrak{h}_{i\neq j} \approx -\chi\frac{\rho}{m\hbar^2}\mathbf{T}_{ij} \tag{40d}$$

In the non-relativistic limit $\mathbf{E} \approx mc^2 \gg \mathbf{p}c \gg \mathbf{p}^2c^2/mc^2$ and hence we get

$$\begin{aligned} &\mathbf{T}_{00} \approx m^2c^4 \\ &\mathbf{T}_{ii} \approx 0 \\ &\mathbf{T}_{i0} \approx 0 \\ &\mathbf{T}_{i\neq j} \approx 0 \end{aligned} \tag{41a}$$

hence

$$\mathrm{T} \approx -m^2c^4 \tag{41b}$$

Moreover if the field is slowly varying with time, the time derivatives on the left hand side of Equation (40) vanish and those equations become:

$$\nabla^2\mathfrak{h}_{00} \approx -\chi\frac{\rho}{\hbar^2}mc^2 \tag{42a}$$

$$\nabla^2\mathfrak{h}_{ii} \approx -\chi\frac{\rho}{\hbar^2}mc^2 \tag{42b}$$

$$\nabla^2\mathfrak{h}_{i0} \approx 0 \tag{42c}$$

$$\nabla^2\mathfrak{h}_{i\neq j} \approx 0 \tag{42d}$$

The above expression for $\mathfrak{h}_{00}$ has to be compared with the expression of the classical gravitation potential $\mathbf{U}$:

$$\nabla^2\mathbf{U} = 4\pi\rho G \tag{43}$$

where G is the gravitation constant. It means that in the non-relativistic limit $\mathfrak{h}_{00}$ is proportional to the Newtonian potential. The constant χ will be hereunder determined by the requirement of compatibility with Newton's equation of motion.

On the other hand, the dynamical equation of a massive particle is given by Equation (27) $\left(\mathfrak{g}^{\mu\nu}\partial_\mu\partial_\nu\right)\Psi - \left(mc/\hbar\right)^2\Psi = 0$ which in the classical limit becomes

$$\mathfrak{g}^{\mu\nu}\mathbf{p}_\mu\mathbf{p}_\nu = -m^2c^2 \tag{44a}$$

or

$$\mathfrak{g}^{00}\mathbf{E}^2 + \sum_{i=1,2,3}\mathfrak{g}^{0i}\mathbf{E}\mathbf{p}_ic + \sum_{i=1,2,3}\mathfrak{g}^{ii}\mathbf{p}_i^2c^2 + \sum_{i\neq j}\mathfrak{g}^{ij}\mathbf{p}_i\mathbf{p}_jc^2 = -m^2c^4 \tag{44b}$$

Let us put

$$\mathfrak{g}^{\mu\nu} = \boldsymbol{\eta}^{\mu\nu} + \mathfrak{f}^{\mu\nu} \tag{45}$$

so that Equation (44b) becomes

$$\left(-1+\mathfrak{f}^{00}\right)\mathbf{E}^2 + \sum_{i=1,2,3}\mathfrak{f}^{0i}\mathbf{E}\mathbf{p}_ic + \sum_{i=1,2,3}\left(1+\mathfrak{f}^{ii}\right)\mathbf{p}_i^2c^2 + \sum_{i\neq j}\mathfrak{f}^{ij}\mathbf{p}_i\mathbf{p}_jc^2 = -m^2c^4 \tag{46a}$$

or

$$\mathbf{E}^2 = \left(m^2c^4 + \mathbf{p}^2c^2\right) + \mathfrak{f}^{00}\mathbf{E}^2 + \sum_{i=1,2,3}\mathfrak{f}^{ii}\mathbf{p}_i{}^2c^2 + \sum_{i=1,2,3}\mathfrak{f}^{0i}\mathbf{E}\mathbf{p}_ic + \sum_{i\neq j}\mathfrak{f}^{ij}\mathbf{p}_i\mathbf{p}_jc^2 \tag{46b}$$

Let us also put

$$\mathbf{E}_{(0)} = \left(m^2c^4 + \mathbf{p}^2c^2\right)^{1/2} \quad (47)$$

We proceed by successive iterations; replacing $\mathbf{E}$ by $\mathbf{E}_{(0)}$ in the right hand side of Equation (46b) gives

$$\mathbf{E}_{(1)}^2 \approx \mathbf{E}_{(0)}^2 + \mathfrak{f}^{00}\mathbf{E}_{(0)}^2 + \sum_{i=1,2,3} \mathfrak{f}^{ii}\mathbf{p}_i^2c^2 + \sum_{i=1,2,3} \mathfrak{f}^{0i}\mathbf{E}_{(0)}\mathbf{p}_i c + \sum_{i \neq j} \mathfrak{f}^{ij}\mathbf{p}_i\mathbf{p}_j c^2 \quad (48a)$$

or

$$\mathbf{E}_{(1)}^2 \approx \mathbf{E}_{(0)}^2 + \mathfrak{f}^{00}m^2c^4 + \sum_{i=1,2,3} \left(\mathfrak{f}^{00} + \mathfrak{f}^{ii}\right)\mathbf{p}_i^2c^2 + \sum_{i=1,2,3} \mathfrak{f}^{0i}mc^2\mathbf{p}_i c + \sum_{i \neq j} \mathfrak{f}^{ij}\mathbf{p}_i\mathbf{p}_j c^2 \quad (48b)$$

In the non-relativistic limit $\mathbf{E} \approx mc^2 \gg \mathbf{p}c \gg \mathbf{p}^2c^2/mc^2$ so that Equation (48b) approximately becomes

$$\mathbf{E}_{(1)}^2 \approx \mathbf{E}_{(0)}^2 + \mathfrak{f}^{00}m^2c^4 \quad (49)$$

Moreover in the weak field limit $\left|\mathfrak{f}^{00}\right| \ll 1$ so that from Equation (49) we finally derive

$$\mathbf{E}_{(0)} \approx mc^2 + \frac{\mathbf{p}^2}{2m} + \frac{\mathfrak{f}^{00}mc^2}{2} \quad (50)$$

If we compare the above expression with the non-relativistic expression

$$\mathbf{E} = mc^2 + \frac{\mathbf{p}^2}{2m} + m\mathbf{U} \quad (51)$$

we see that the particle is undergoing an effective gravitation potential

$$\mathbf{U} = \mathfrak{f}^{00}c^2/2 \quad (52a)$$

Since $\mathfrak{g}^{\mu\nu}\mathfrak{g}_{\mu\nu} = \mathbf{I}$ this is equivalent to

$$\mathbf{U} = -\mathfrak{h}_{00}c^2/2 \quad (52b)$$

Since from Equation (42a) $\nabla^2\mathfrak{h}_{00} \approx -\chi\frac{\rho}{\hbar^2}mc^2$ the above expression of $\mathbf{U}$ yields

$$\nabla^2\mathbf{U} \approx \chi\frac{\rho mc^4}{2\hbar^2} \quad (53)$$

By comparison with the expression of the classical gravitation potential $\nabla^2\mathbf{U} = 4\pi\rho G$ we get

$$\chi = \frac{8\pi G\hbar^2}{mc^4} \quad (54)$$

If we had retained the $\lambda^2\mathfrak{g}^{\alpha\beta}\mathfrak{g}_{\alpha\beta}$ term in the expression Equation (30) of the Lagrangian density of the gravitation field, we would have in Equation (52b) an additional constant term; the comparison with the classical gravitation potential implies $\lambda = 0$. The field equation Equation (37) now writes as

$$\left(2\mathfrak{g}_{\mu\alpha}\mathfrak{g}_{\nu\beta} - \mathfrak{g}_{\mu\nu}\mathfrak{g}_{\alpha\beta}\right)\left(\mathfrak{g}^{\rho\sigma}\partial_\rho\partial_\sigma\mathfrak{g}^{\alpha\beta}\right) = -\frac{16\pi\rho G}{m^2c^4}\boldsymbol{\tau}_{\mu\nu} \quad (55)$$

5. Post-Newtonian Terms

From the expressions Equation (42) we derive in the weak, slowly varying field limit

$$\mathfrak{g}_{00} \approx -1 - 2\frac{\mathbf{U}}{c^2} \quad (56a)$$

$$\mathfrak{g}_{ii} \approx 1 - 2\frac{\mathbf{U}}{c^2} \quad (56b)$$

$$\mathfrak{g}_{0i} \approx 0 \quad (56c)$$

$$\mathfrak{g}_{i \neq j} \approx 0 \quad (56d)$$

so that

$$\mathrm{d}s^2 \approx -\left(1+2\frac{\mathbf{U}}{c^2}\right)c^2\mathrm{d}t^2 + \left(1-2\frac{\mathbf{U}}{c^2}\right)\left(\mathrm{d}x^2+\mathrm{d}y^2+\mathrm{d}z^2\right) \quad (57)$$

In addition, Equation (48b) gives

$$\mathbf{E}_{(1)}^2 \approx \mathbf{E}_{(0)}^2 + 2m^2c^2\mathbf{U} + 4\frac{\mathbf{U}}{c^2}\mathbf{p}^2c^2 \quad (58)$$

This has to be compared with the Newtonian expression at the lowest order in $\mathbf{p}^2c^2$ and $m\mathbf{U}$

$$\mathbf{E}^2 = m^2c^4 + \mathbf{p}^2c^2 + 2m^2c^2\mathbf{U} + \frac{\mathbf{U}}{c^2}\mathbf{p}^2c^2 + o\left(m^2\mathbf{U}^2, \mathbf{p}^4c^4\right) \quad (59a)$$

or

$$\mathbf{E}^2 \approx \mathbf{E}_{(0)}^2 + 2m^2c^2\mathbf{U} + \frac{\mathbf{U}}{c^2}\mathbf{p}^2c^2 \quad (59b)$$

6. Conclusions

Introducing the Planck length $L_P = \left(\hbar c^{-3}G\right)^{1/2}$ and the Planck mass $M_P = \left(\hbar c G^{-1}\right)^{1/2}$ leads to the following expression for the full Lagrangian density of the (field + particle) system

$$\mathcal{L} = \left[\mathfrak{g}^{\rho\sigma}\partial_\rho\mathbf{\Psi}^\dagger\partial_\sigma\mathbf{\Psi} + \left(mc/\hbar\right)^2\mathbf{\Psi}^\dagger\mathbf{\Psi}\right] - \frac{1}{8\pi}\frac{m}{M_P}\frac{1}{L_P^3}\left[\mathfrak{g}^{\mu\nu}\left(\mathfrak{g}_{\alpha\rho}\partial_\mu\mathfrak{g}^{\rho\beta}\right)\left(\mathfrak{g}_{\beta\sigma}\partial_\nu\mathfrak{g}^{\sigma\alpha}\right)\right] \quad (60)$$

$\left(M_P \approx 2.17651\times10^{-8}\ \text{kg}\right)$. According to that expression, the physical objects such as $m \ll M_P$ have their dynamics mainly driven by the forces other than gravitation and the effective space-time metrics $\mathfrak{g}$ is the metrics generated by the external masses. For the objects such as $m \gg M_P$, gravitation is a major driver of their dynamics, and they generate the gravitation field as well as they undergo it.

The usual approach of general relativity is most adequate for describing the universe on a large scale in astrophysics and cosmology. The approach of this paper, derived from particle physics and focused on local reference frames, underlines the formal similarity between gravitation and the other interactions inasmuch as they are associated to the restriction of a global symmetry to a local one.

In a 10-dimension space-time as it is considered in certain unification theories, gravitation is linked to the geometry of the 4 usual dimensions whereas the other fundamental interactions can be associated to the geometry of the 6 additional ones; in that approach extra fields (which eventually may account for dark matter and/or dark energy) naturally come out by regarding the geometry of the full 10-dimension set.

References

[1] Landau, L. and Lifshitz, E. (1966) Field Theory. Mir Editions, Moscow.

[2] Weinberg, S. (1972) Gravitation and Cosmology. John Wiley, Hoboken.

[3] Lanczos, C. (1949) Lagrangian Multiplier and Riemannian Spaces. *Reviews of Modern Physics*, **21**, 497. http://dx.doi.org/10.1103/RevModPhys.21.497

[4] Takeno, H. (1964) On the Spin Tensor of Lanczos. *Tensor*, **15**, 103.

[5] Ivanenko, D. and Sardanashvili, G. (1983) The Gauge Treatment of Gravity. *Physics Report*, **94**, 1-45.

[6] Lasenby, A., Doran, C. and Gull, S. (1998) Gauge Theories and Geometric Algebra. *Philosophical Transactions of the Royal Society*, **A356**, 487-582. http://dx.doi.org/10.1098/rsta.1998.0178

[7] Blagojevic, M. and Hehl, F.W. (2013) Gauge Theories of Gravitation: A Reader with Commentaries. World Scientific, Singapore. http://dx.doi.org/10.1142/p781

[8] Becchi, C. (1997) Introduction to Gauge Theories. arXiv:hep-ph/9705211v1

[9] Mann, R. (2010) An Introduction to Particle Physics and the Standard Model. CRC Press, Boca Raton.

[10] Roll, P.G., Krotkov, R. and Dicke, R.H. (1964) The Equivalence of Inertial and Passive Gravitational Mass. *Annals of Physics*, **26**, 442-517.

Natural Science, 2014, 6, 1253-1258
Published Online November 2014 in SciRes. http://www.scirp.org/journal/ns
http://dx.doi.org/10.4236/ns.2014.616114

A New 3D Surface Profile Measuring System Based on the Telescope and Webcam

Ming-Hung Chiu*, Yen-Hsin Chen, Jian-Ming Su

Department of Electro-Optical Engineering, National Formosa University, Taiwan
Email: *mhchiu@nfu.edu.tw

Received 17 September 2014; revised 28 September 2014; accepted 12 October 2014

Abstract

We propose a simple telescope with three-dimensional image capability for surface profile measurements. Our method based on the algorithm of reflectivity-height transformation is applied to a traditional commercial telescope with a webcam for determining the third dimension of the test object. It is also useful for thickness, deformation, and surface profile measurements.

Keywords

Telescope, Three-Dimensional Measurement, Reflectivity, CCD, Webcam, Surface Profile

1. Introduction

In recent decades, telescopes have not undergone any major variations in their structures or applications. A picture from a telescope can be taken by a camera. We can take a picture in two-dimensional (2D) but not in three-dimensional (3D) format. In this paper, we propose a new telescope that has the ability to show and plot a 3D image for long distance surface profile measurements. The method is based on the reflectivity-height transformation, including the internal reflection effect [1] of a prism and the principles of the first-order optics. The difference of intensity or reflectance is proportional to the object distance and the deviation angle of the light. We have previously proposed 3D profilometers for both the transmission [2] and reflection [3] types, but they were applied for measuring smooth surface profiles of small areas or for use with a microscope. The method had been demonstrated and used in biological measurements [4]. The main structure of our 3D telescope combines a commercial telescope with a webcam and a parallelogram prism. These components are inexpensive and can be easily acquired. The experimental results of several coins have shown that the error percentage of thickness can be less than 4% for a telescope with a magnification of 25× and a measuring distance of 10 m. It will be applicable for remote measurements in the future.

*Corresponding author.

How to cite this paper: Chiu, M.-H., Chen, Y.-H. and Su, J.-M. (2014) A New 3D Surface Profile Measuring System Based on the Telescope and Webcam. *Natural Science*, **6**, 1253-1258. http://dx.doi.org/10.4236/ns.2014.616114

2. Method: Reflectivity-Height Transformation

When a parallelogram prism made of BK7 with the base angle of 45˚ is used to be an angular sensor to sense the angle deviation of the object light, the light passing through it with twice internal reflections. n_1 and n_2 are the indices of refraction of the prism and air respectively. Assume that n_2 = 1.000 and n_1 = 1.517 (the average wavelength λ = 550 nm), and the range of external incident angle θ = 0˚ - 10˚. The simulation results of the reflectivities of the *s*- and *p*-polarized lights are shown in **Figure 1(a)**, where R_{s2} and R_{p2} are represented the reflectivities of twice internal reflection of the *s*- and *p*-polarized lights, respectively. Apparently, the change in the reflectivity of the *p*-polarized light (dotted line) close to the critical angle is more sensitive than that of the *s*-polarized light (solid line) close to the critical angel.

Regarding objects with a large change in height, we can prefer to select the *s*-polarized light as the light source because of its larger angle measurement range. Convert the practical measured curve into coordinates, where the x-coordinate is converted to R_{S2}, y-coordinate is converted to θ, and convert the angle θ to be the function of R_{S2}, as shown in **Figure 1(b)**.

From **Figure 1(a)**, the change of θ will result in the change of R_{s2}; on the contrary, we can derive the change of θ from the change of R_{s2}, as shown in **Figure 1(b)**. As a result, we receive the images from the webcam to record the light intensities of the incident angles close to the critical angle and the total reflection (TIR) respectively, and then use Matlab software to overlap the two images and calculate the reflectivity R_{s2}. When the interval of the two points of the object is Δx, the reflection lights are projected into the parallelogram prism and then passed via a telescope to form the image on the webcam; the interval of the two points of the formed image correspond to Δx is ΔX. If we take ΔX as the interval of the adjacent two pixels of the webcam, we can derive Δx via the optical magnifying power. As shown in **Figure 2**, the two points have different heights, and the tilt angle is α; thus, the difference in the reflection angles of the two points is 2α; if α is very small, the height difference between the two points can be expressed as:

$$\Delta h = \tan\alpha\Delta x \approx \alpha\Delta x, \tag{1}$$

If we can acquire the reflectivity difference R_{s2} of the two points after imaging and calculate $\Delta\theta$ via the function shown in **Figure 1(b)**, we can derive α via the optical magnifying power MP.

As $\Delta x = \Delta X / MP$ and $\alpha = MP\Delta\theta/2$, we can substitute them into Equation (1). The height difference can be rewritten as

$$\Delta h = \frac{\Delta\theta}{2}\Delta X = K\Delta\theta, \tag{2}$$

where $K = \Delta X/2$ is a constant and if the tilt angle α is very small, *i.e.* $\Delta\theta \to 0$, then $\Delta\theta$ can be written as $\mathrm{d}\theta$, we can integrate them into the Equation (2), thus the surface height could be given as

$$h = \int K\mathrm{d}\theta = K\theta + h_0, \tag{3}$$

where h_0 is the initial height.

3. Experimental Results

The system structure of the experiment is shown in **Figure 3**, and the object to be tested (1) is placed right in front of the telescope. The light source used in the experiment is a fluorescent lamp (2) (the average wavelength = 550 nm). When the object is placed far away from the system, it can be considered a parallel light, which will pass through device (3) (Polarizer). The transmission axis of the polarizer should be adjusted to 90 degrees to make sure that all received lights are the *s*-polarized lights. Afterward, the beam passes through device (4) (filter plate) and only green lights with specific wavelengths can pass through device (4). Next, device (5) (parallelogram prism) is rotated by device (6) (rotation platform) until the angle of device (5) reaches the TIR angle and critical angle that is needed. Then, we can conduct observation using device (7) (telescope). Finally, we use device (8) (the image capturing unit, such as a webcam, or CCD) to capture images of the TIR and the critical angle, and then process and analyze them by device (9) (personal computer (PC) with Matlab software) to calculate the reflectivity R_{s2} and h, where $\Delta R_{s2} \doteqdot \mathrm{d}R_{s2}$ can be considered the reflectivity difference of the adjacent pixels and $\mathrm{d}X$ can be considered the interval of the adjacent pixels. According to Equation (3), the surface height of object can be calculated and the 3D surface profile can be plotted.

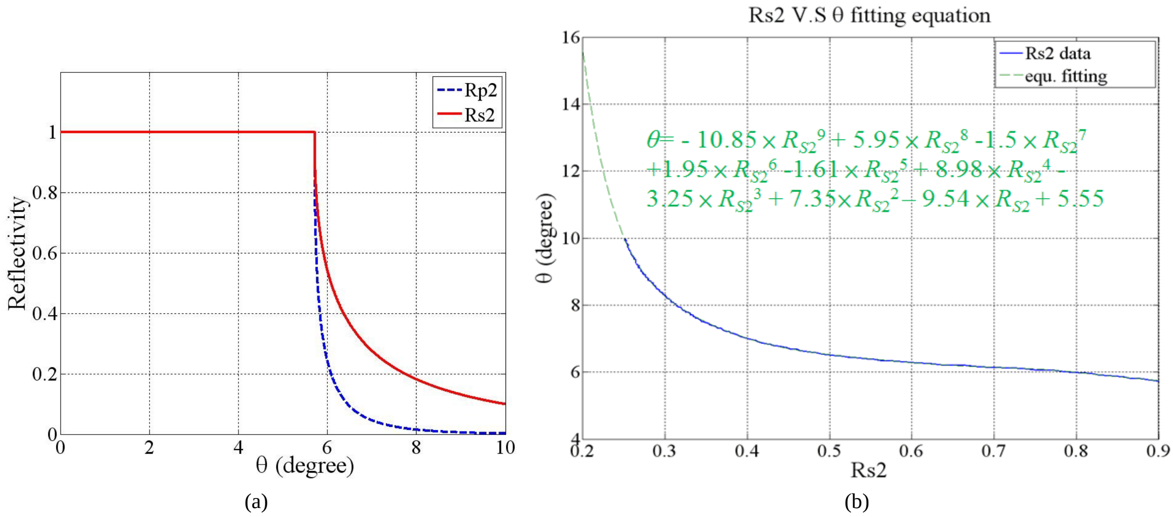

Figure 1. (a) A simulation of the changes of the reflectivities of the twice internal reflections of the *p*- and *s*-polarized lights to the external angle; (b) The practical measured equation and relation curve of external angle θ versus reflectivity R_{s2} after the coordinates converted.

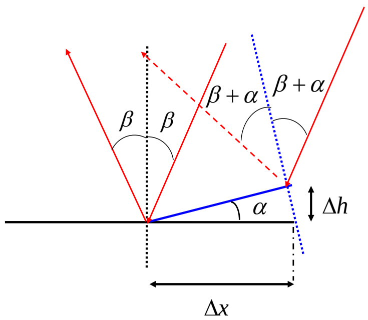

Figure 2. When the tilt angle of two adjacent points on the object is α, the change in the reflection angle will be 2α.

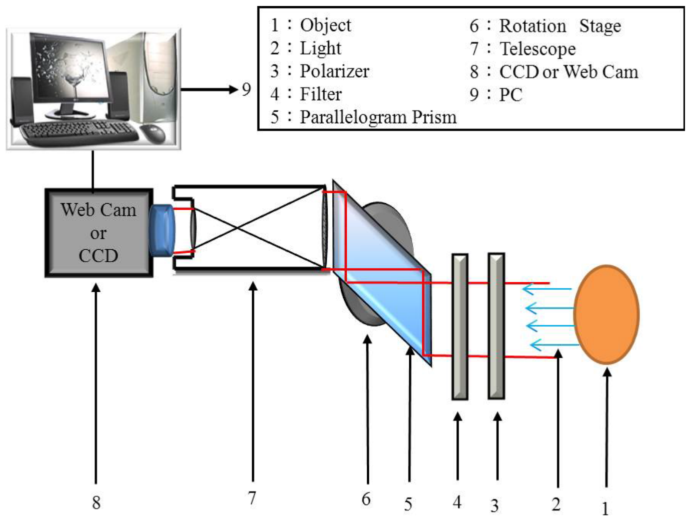

Figure 3. System structure diagram.

In order to measure more accurate 3D surface profiles, we need to use a green filter plate to perform the measurement. As described above, after we perform curve fitting for obtaining the external incident angle θ, we can finally obtain the 3D surface profile of the object. In one of our experiments, two objects to be tested together are a key and an Australian coin and they are away from the system by 10 m. First, we measure the width and thickness of the samples using a vernier caliper. The width of the key is 18.99 mm and its thickness is 1.72 mm; the width of the Australian coin is 23.6 mm and its thickness is 1.7 mm. **Figure 4(a)** shows the 3D surface profiles of the key and the Australian coin; the height of the higher part is about 2.09 mm and the height of the lower part (recession) is about 1.13 mm, as shown in **Figure 4(b)**, and the length of the key is about 53.62 mm. The points marked in **Figure 4(a)** are the heights of the human portrait or the words protruding from the surface of the coin and the recession of the object to be tested. These show that the heights of point A, B, C, D, are 1.13, 2.22, 2.26 and 1.248 mm, respectively.

In addition to the above experiment, we also performed experiments on other coins to make sure the proposed method is feasible and to find out the average error range. We compared the average thickness with the measurement results of the vernier caliper. The measurement results of the vernier caliper serve as the reference values. The error of the thickness is about 0.07 mm and the average error percentage is 4%. According to first-order optics approximation, as the measurement distance of the structure is 10 m, the *f*-number is 5.346, and the diameter of telescope is 52 mm, the corresponding depth of field is 31 mm, the object range that we measured cannot exceed the limit [5].

4. Discussions

The definition of the sensitivity S is written as

$$S = \left|\frac{\partial R_S}{\partial h}\right| \tag{4}$$

∂R_S is the reflectivity change corresponding to the micro height change. The highest sensitivity and the lowest sensitivity with a measurement range of 5.8˚ - 8.5˚ When the external angle is 5.8˚, we find that the highest sensitivity S = 0.41 (change/mm); when the external angle is 8.5˚, we find that the lowest sensitivity S = 0.07 (change/mm).

Vertical resolution means the minimal surface height which the system can discriminate. Where S is the sensitivity, $\Delta R_{s2}(\min)$ is the minimal reflectivity change which the CCD can discriminate, and the expression method of the gray level value of the CCD is 0 - 255, for 8 bits A/D converter, the vertical resolution can be defined by the following equation

$$R_V = \frac{\Delta R_{S2}(\min)}{S} \tag{5}$$

The vertical resolution of the system is shown in **Figure 5**; when the external angle is 7.2˚, the vertical resolution is 33.73 μm.

The light source is an indoor fluorescent lamp, so the experiment does not need to be conducted in a dark room. Thus, we not only need to consider the stability of the power of the fluorescent lamp, but we also need to consider whether the system receives light from other sources in order to be aware of any measurement errors. Regarding the stability of the light source, we use the power meter to continuously measure the stability of fluorescent lamp, as shown in **Figure 6**:

As shown in **Figure 6**, the number of the sampling points of the x-coordinate is 400, and the sampling frequency is 0.25 times per second; the power unit of the y-coordinate is μW. We can see the average optical power of the fluorescent lamp is 134.7 μW, and its swaying quantity is about ±0.06 μW. Therefore, we know that the swaying quantity of the fluorescent lamp is about 0.04%. For using the 8 bits A/D converter, the CCD's gray level is in the region of 0 - 255, the minimal discriminable change is about 0.4%. As the light intensity change of the fluorescent lamp is lower than 0.4%, it will not influence the best light intensity resolution of the CCD; accordingly, we can let $\Delta R_{s2}(\min) = 1/256$.

Lateral resolution means the minimal discriminable interval. According to the Rayleigh Criterion, $R_l = L \times 1.22\lambda/D$, where L is the distance of the target to be measured, and D is the aperture of the telescope (or the effective light collection of the system). Accordingly, we know that the lateral resolution is determined by the measurement distance L and the aperture D. When we increase the measurement distance, the minimal discriminable distance will increase; in other words, the lateral resolution will be reduced. On the other

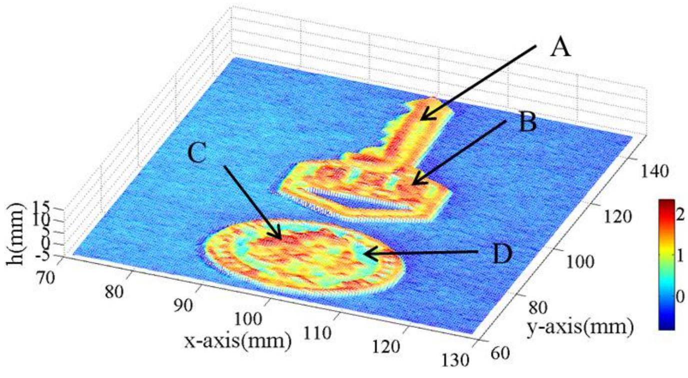

(a)

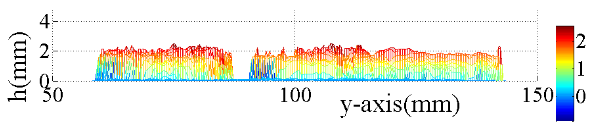

(b)

Figure 4. (a) The 3D surface profiles of the key and the Australian coin; (b) The height diagram of the key and the Australian coin.

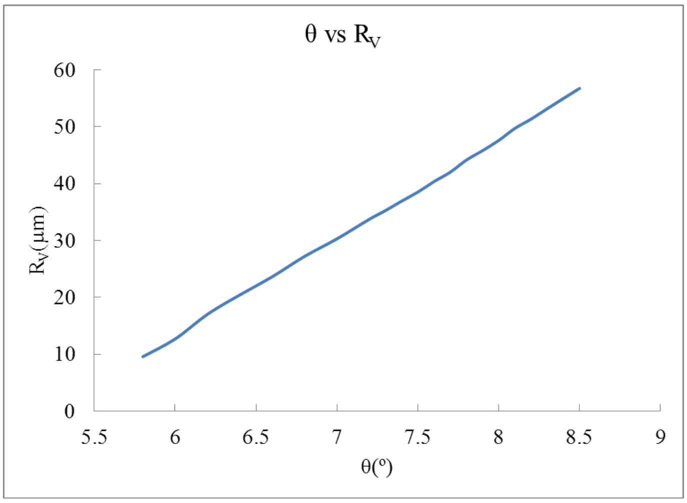

Figure 5. A curve diagram of the vertical resolution in response to the external angle change.

hand, if the effective light collection aperture is smaller, the minimal discriminable distance will also increase and the lateral resolution will be reduced. If we want to improve the lateral resolution, we can use a telescope with a bigger aperture; that is to say, we increase to improve the lateral resolution. With the telescope that we currently use, D = 52 mm, the measurement distance is 10 m, and the lateral resolution is 0.13 mm.

5. Conclusion

This experiment adopts the angle deviation method by using the parallelogram prism, common telescope and webcam to measure the 3D surface profiles of coins with a thickness of several millimeters at a 10 m distance. The error percentage is about 4%. According to reflectivity-height transformation, this method converts the reflectivity into the height of the object point by point, and then acquires its 3D surface profile in real time. Thus, the device can be used for remotely monitoring or detecting the change of the surface profile. Examples include measuring a change in topography with aerial photos, monitoring dangerous or inaccessible environments, ob-

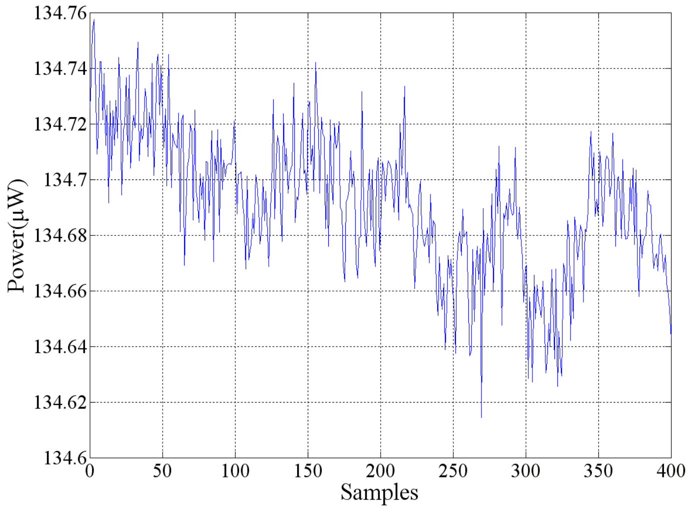

Figure 6. A stability diagram of the power of the fluorescent lamp as measured by the power meter.

serving the cracks or deformation of buildings, investigating soil flows or floods, and remote testing for other purposes.

Acknowledgements

This study was supported in part by the National Science Council of Taiwan with contract number NSC 100-2221-E-150-067-MY2.

References

[1] Born, M. and Wolf, E. (1999) Principles of Optics. 7th Edition, University of Cambridge, Cambridge, 38-52. http://dx.doi.org/10.1017/CBO9781139644181

[2] Tan, C.T., Chan, Y.S., Lin, Z.C. and Chiu, M.H. (2011) Angle-Deviation Optical Profilometer. *Chinese Optics Letters*, **9**, Article ID: 011201. http://www.opticsinfobase.org/col/abstract.cfm?uri=col-9-1-011201

[3] Tan, C.T., Chan, Y.S., Chen, J.A., Liao, T.C. and Chiu, M.H. (2011) Non-Scanning, Non-Interferometric, Three-Dimendional Optical Profilometer with Nanometer Resolution. *Chinese Optics Letters*, **9**, Article ID: 101202. http://www.col.org.cn/abstract.aspx?id=COL201109101202-03

[4] Chiu, M.H., Tan, C.T., Lee, T.S. and Lee, J.C. (2013) Non-Scanning Three Dimensional Optical Microscope Based on the Reflectivity-Height Transformation for Biological Measurements. *Microscopy & Microanalysis*, **19**, 425-432. http://dx.doi.org/10.1017/S1431927612014365

[5] Greivenkamp, J.E. (2004) Field Guide to Geometrical Optics. 1st Edition, SPIE Press, Bellingham, 35-36. http://dx.doi.org/10.1117/3.547461.p35

Natural Science, 2014, 6, 1259-1265
Published Online November 2014 in SciRes. http://www.scirp.org/journal/ns
http://dx.doi.org/10.4236/ns.2014.616115

Scientific Research

The Gap Labelling Integrated Density of States for a Quasi Crystal Universe Is Identical to the Observed 4.5 Percent Ordinary Energy Density of the Cosmos

Mohamed S. El Naschie

Department of Physics, University of Alexandria, Alexandria, Egypt
Email: Chaossf@aol.com

Received 30 August 2014; revised 29 September 2014; accepted 15 October 2014

Academic Editor: Leila Marek-Crnjac, Technical School Center of Maribor, Slovenia

Abstract

Condense matter methods and mathematical models used in solving problems in solid state physics are transformed to high energy quantum cosmology in order to estimate the magnitude of the missing dark energy of the universe. Looking at the problem from this novel viewpoint was rewarded by a rather unexpected result, namely that the gap labelling method of integrated density of states for three dimensional icosahedral quasicrystals is identical to the previously measured and theoretically concluded ordinary energy density of the universe, namely a mere 4.5 percent of Einstein's energy density, *i.e.* $E(O) = mc^2/22$ where E is the energy, m is the mass and c is the speed of light. Consequently we conclude that the missing dark energy density must be $E(D) = 1 - E(O) = mc^2(21/22)$ in agreement with all known cosmological measurements and observations. This result could also be interpreted as a strong evidence for the self similarity of the geometry of spacetime, which is an expression of its basic fractal nature.

Keywords

E-Infinity Theory, Fractal-Witten M-Theory, Gap Labelling Theorem, Density of States, Dark Energy Density, Noncommutative Geometry, K-Theory, Dimension Group

1. Introduction

It is well known that many models and mathematical techniques that proved to be valuable in the low energy

How to cite this paper: El Naschie, M.S. (2014) The Gap Labelling Integrated Density of States for a Quasi Crystal Universe Is Identical to the Observed 4.5 Percent Ordinary Energy Density of the Cosmos. *Natural Science*, **6**, 1259-1265.
http://dx.doi.org/10.4236/ns.2014.616115

domain of condense matter physics were found to be of considerable usefulness in clarifying basic questions in high energy physics [1]-[7]. Symmetry breaking and phase transition [3] are well known examples for the above, which resulted in the major discovery of the Higgs boson [4]. The hypothesis is also well known that the universe is a gigantic self similar structure [6] [7] as partially evidenced by the planetary system of the Rutherford-Bohr atom model [5]. Nevertheless the result of the present paper goes far beyond what the preceding fact could have led us to believe and it was rather a delightful unexpected result to find that the methods of solid state physics and the suspected self similarity of a fractal universe [6] [7] could lead to accurate results setting the gap labelling integrated density of states for a 3-D quasicrystals [8]-[12] equal to the ordinary energy density of the cosmos as found by COBE, WMAP and the Planck measurements [13]-[18]. In fact these various accurate measurements which lead to several Nobel prizes in physics [13]-[20] are in complete accordance with the theoretical results obtained in the last three years or so [21]-[25] and in turn these theoretical energy density derivations give identical results to the present one [16]-[25] as will be expanded upon in the following sections. In short the main objective of the present paper is to show that the methods of high energy physics and that of low energy solid state physics converge in a clear way leading to the same dark energy density.

2. Integrated Density of States

2.1. Background Information

It is well known that electronic band theory is a very useful and successful theory in the physics of solids that solved difficult problems connected to the design of solar cells and transistors as well as illuminating fundamental properties of solids such as optical absorption and electrical resistance [8]. In this respect the density of states and the Brillouin zone plays a central role [8]. Thus the said density function is defined as the number of electronic states per unit energy for nearby electron energy while the Brillouin zone is polyhedron in Schrödinger wave vector space, which is related to a corresponding crystal lattice [8]-[12].

Now with a somewhat unconventional but well motivated idea in the back of our minds, namely that of drawing an instructive analogy between the zero density inside a band gap and the geometry and topology of the crystal lattice on the one side and ordinary energy and dark energy density contained in the structure of our cosmos on the other side, we will start here by extending the above concepts and notions to quasi periodic crystalline [8] [10] [11]. Luckily we already have at our disposal a gap labelling theorem to lean on as well as many results obtained notably by J. Bellisard [8], A. Connes and many others who applied the powerful mathematical machinery of K-theory and noncommutative geometry [26] to the problem. For example an extensively used standard model is the Fibonacci sequence of two letters a and b in which the frequency of the "a" is given by the golden mean [8] [11]. This we consider next.

2.2. Gap Labelling Density of States of One Dimensional Discrete System

Probably the simplest group of one dimensional systems to illustrate the theory at hand is an automatic sequences such as period doubling, the Rudin-Shapiro sequence and Thue-Morse sequence [8]. However the Fibonacci sequence is the most appropriate for our purpose here not only because it is the simplest but also because it constitutes in the limit a one dimensional Cantorian space with a Hausdorff dimension equal $d_{(c)}^{0}=\left(\sqrt{5}-1\right)/2$ and a Menger-Urysohn topological dimension $n=-1$ while displaying a remarkable integrated density of states having the same information as that of a higher dimensional model. Let the two letters alphabet be given by $A=\{0,1\}$ and let the substitution be

$$\begin{aligned} y(0)&=01 \\ y(1)&=0 \end{aligned} \tag{1}$$

Following Bellissard's general exposition and his notation we find two matrices [8]

$$M(y)=\begin{bmatrix}1 & 1\\ 1 & 0\end{bmatrix} \tag{2}$$

and

$$M_2(y)=\begin{bmatrix} 0 & 0 & 1 \\ 1 & 1 & 0 \\ 1 & 1 & 0 \end{bmatrix} \tag{3}$$

The largest Eigenvalue of the above is $P=\left(\sqrt{5}+1\right)/2$, *i.e.* $P=1/\phi$ where $\phi=\left(\sqrt{5}-1\right)/2$ is the golden mean. Using the same notation and abbreviations of [8] the corresponding Eigenvectors are consequently

$$V=\begin{bmatrix} \phi \\ 1-\phi \end{bmatrix}$$

$$V_2=\begin{bmatrix} 2\phi-1 \\ 1-\phi \\ 1-\phi \end{bmatrix} \tag{4}$$

and the integrated density of states (IDS) is given by [8]

$$[\mathrm{IDS}]=a+b\phi \tag{5}$$

where $a,b\in Z$. It is almost impossible for anyone familiar with noncommutative geometry or E-infinity theory to overlook that the preceding density is at a minimum formally identical to that of the compactified Penrose tiling dimensional function [7] [11] [26] as well as the bijection formula of Cantorian spacetime [7] [26] [27]. Thus as simple as the preceding analysis may be, it has far reaching consequences which we discuss next in the context of a K-analysis of the famous Penrose fractal tiling [11] [12] [26].

2.3. Landi's K-Analysis of the Penrose Tiling

As noted by Landi [12], the K-theory of Penrose universe treated as x-space by Connes [26] is straight forward and leads via Bratteli diagram and the fact that {0} is the only primitive ideal to the inclusion [12]

$$\mathrm{In}: A_n \Rightarrow A_{n+1} \tag{6}$$

which is reminiscent of the previous recursive Fibonacci example. Proceeding in the usual way Landi can then prove the proposition that the *c* star algebra of the Penrose tiling gives rise to a group given by [12]

$$K_o=Z\oplus Z \tag{7}$$

and

$$K_{o+}=\left\{(a,b)\in Z\varnothing Z;\ a+\phi b\geq o\right\} \tag{8}$$

This result is again identical to that obtained by Connes and noting the one to one correspondence between the bijection formula of E-infinity Cantorian spacetime [7] [19] [26]-[29]

$$d_c^{(n)}=(1/\phi)^{n-1} \tag{9}$$

and von Neumann-Connes dimensional function it follows that k_{o+} as well as [IDS] are simply mathematical tautology, albeit an extremely instructive one bringing various theories for the micro cosmos and the large structure of spacetime [29] to come together and reveal their quintessentially identical nature. One must add however that the bijection formula is a far more compact notation and one could deduce $d_c^{(n)}$ for negative dimensions much easier than by using the recursive Fibonacci prescription of K-theory and noncommutative geometry. Thus for the empty set we see immediately that $n=-1$ leads to [7] [27]

$$d_c^{(-1)}=(1/\phi)^{-1-1}=(1/\phi)^{-2}=\phi^2 \tag{10}$$

exactly as should be while the zero set is given clearly by [7] [27]

$$d_c^{(0)}=(1/\phi)^{0-1}=(1/\phi)^{-1}=\phi \tag{11}$$

so that $d_c^{(-1)}+d_c^{(0)}=\phi+\phi^2=1$ is nothing but our unit set [7] [27]

$$d_c^{(1)} = (1/\phi)^{1-1} = (1/\phi)^0 = 1 \tag{12}$$

Next we discuss the vital physical and cosmological implication of the preceding results.

3. Ordinary and Dark Energy from Integrated Density of States and Gap Labelling

One of the most important conclusions arrived at from the preceding Section 2 is that what we called topological probability ϕ^n are also Hausdorff dimensions for negative Menger-Urysohn space [7] [27] and consequently the inverse of a Hausdorff dimension of a corresponding positive dimension n. Actually we have known this fact since a long time from our work on E-infinity [7] [27]. However the slightly new twist is that these normed Hausdorff dimensions or probability corresponds to a subtle form of geometrical density with a physical meaning. To explain what we mean in a more direct and specific way we could do nothing better than derive the celebrated Hardy's probability for quantum entanglement [19]-[22] and proceed from there to the computation of the ordinary and the dark energy density of our universe and discuss its direct interpretation as an integrated density of states [8] which implies that our cosmos is akin to a gigantic quasi crystalline with Cantorian fine structure.

Hardy's quantum probability of entanglement [19]-[22] is an ideal starting point for various very good reasons. First it is an exact solution of two quantum particles using orthodox quantum mechanics a la Dirac [19]-[22]. Second this exact solution turned out to be a most surprizing quantitative answer with a strong qualitative flavour being the golden mean ϕ to the power of five, that is to say

$$P(\text{Hardy}) = \phi^5 = \left[\left(\sqrt{5}-1\right)/2\right]^5 = 0.09016994393 \tag{13}$$

Being a probability we could look upon it as being the inverse of a dimension, *i.e.* un-normed probability given by the bijection formula [7] [27]. Taking the dimensionality n to be $n = 6$ one finds [7] [27] [19]-[22]

$$d_c^{(6)} = (1/\phi)^{6-1} = (1/\phi)^5 = 11 + \phi^5 = 11 + \cfrac{1}{11 + \cfrac{1}{11 + \cdots}} \tag{14}$$

Therefore we have the normed probability [19]-[22]

$$1/d_c^{(6)} = 1/\left(11 + \phi^5\right) = \phi^5 = P(\text{Hardy}) \tag{15}$$

Alternatively we could see P(Hardy) as living in a negative four dimensional space $n = -4$ which leads to [7] [27]

$$d_c^{(-4)} = (1/\phi)^{-4-1} = \phi^5 \tag{16}$$

Here we tacitly made use of the notion of the degree of emptiness of an empty set introduced first by the late inventor of the word fractals, B. Mandelbrot [7]. This is so because the zero set $n = 0$ is the surface of the empty set $n = -1$ while the empty set $n = -1$ is the surface of an emptier still set $n = -2$. Similarly $n = -2$ is the surface of $n = -3$ and $n = -3$ is the surface of $n = -4$ and so on add infinitum until we reach, via the philosophical concept of infinity, the dual philosophical concept of a true insubstantial nothingness [7] [27].

Let us return to $d_c^{(6)}$ and in particular ponder the meaning of its continued fraction. The geometry of continued fractions is a specialized and rich subject in its own right [30]-[32]. Here we mention only on passing the geometrical relevance of continued fractions in connection with SL(2, 7) Lie symmetry groups of which the holographic boundary of E-infinity theory, *i.e.* SL(2, 7) is a member as well as the density points theorems on measurable subsets and multi-dimensional continued fractions [32]. However our main attention should be placed on the appearance of the remarkable prime number eleven of super gravity and Witten's M-theory [33]-[36]. Even in the simple form given here it is obvious that $11 + \phi^5$ represents a self-similar fractal-like version of the original M-theory spacetime (see [33] Figure 1 and Figure 2 as well as [36] Figure 3). It is easily reasoned that $11 + \phi^5$ is equal to the isomorphic length of a super symmetric space [33] [36], made of the bosonic $D = n = 4 + \phi^3$ and fermionic $D = n = 5 + \phi^3$ of E-infinity theory [19]-[21]. The intersection of both spaces gives us therefore a super symmetric space with $D = n = \left(4 + \phi^3\right)\left(5 + \phi^3\right) = 22 + 2\phi^5$ where $2\phi^5$ is equal to $k = \phi^3\left(1 - \phi^3\right) = \in$ of "tHooft-Veltman-Wilson" dimensional regularization [35]. Seen that way $D = n = 22 + k$ becomes not only a Hausdorff dimension but a measure for the ordinary energy density of our universe, namely

[13] [16]-[25] [33]-[36]

$$E = E(\text{Einstein})/(22+k) = mc^2/(22.18033989) \cong mc^2/22 \tag{17}$$

where the 22 may be viewed as the compactified dimensional subset of the 26 dimensions of the bosonic string theory [19]-[21]. In other words, for a normed $m = 1$, $c = 1$ we have $E(\text{Einstein}) = 1$ and the measurable energy density is simply $1/D = 1/(22+k) \simeq 1/22 \cong 95.5$ percent in full agreement with all actual cosmic measurements and observations [15]-[25]. Looking now at the entire situation in a global manner we could see not only that the very same mathematics which is developed for the very small is also applicable seamlessly to the extremely large but also that the physics underneath is quite similar. A band gap is evidently where a density of states function is equal zero [8]. In our spacetime model this could play the role of the empty set [33] [34]. The electrons on the other hand represent the analogue of the zero set. This is in fact quite reasonable from the viewpoint of fractal logic and the fractal counting of photons, which are the messenger particles, connected to the fermionic electron and which has a fractal weight number equal ϕ rather than one. Consequently the electrons will correspond to Cantorian dust responsible for the ordinary measurable energy density [17]-[25].

4. Conclusions

There is one aspect of theoretical physics that is so incredibly beautiful that one cannot find the right words to describe it. This is a first hand experience of the present author which happens whenever he notices that two totally different fields can be directly connected and analogies established simply because the same stringent logic, *i.e.* the same mathematical pattern and schemes are obeyed by both fields. One such case is the connection between super conductivity and the high energy physics of elementary particles [1]-[4]. This is truly the unreasonable effectiveness of mathematics which on deeper still reflection, is truly reasonable.

The present work reveals a similar situation where the extremely small and large ultra obeys basically the same subgroup of R generated by Z and the golden mean number ϕ so that the density or the frequency of appearance of a motive by certain tiling, in our case Klein-Penrose fractal universe, by virtue of the basic topology must be an element of the dimensional group given by von Neumann-Connes dimensional function [11] [12] [26] [27] or equivalently the K- and E-theory bijection formula [7] [8] [12] [26] [27]. In all cases it turns out that the probability of finding a Cantorian point in the fractal M-theory space which has a Hausdorff dimension equal to 11 plus Hardy's quantum entanglement, *i.e.* $11+\phi^5$ is given simply by the inverse value of this dimension, *i.e.* $1/(11+\phi^5) = \phi^5$ [33] [34]. Since such a 'point' is super symmetric by definition, it is a double point and ϕ^5 should be divided by $n = 2$ to give us the net value corresponding to a single "Cantorian" [27]. We have shown here, in accordance with earlier derivations, that $\phi^5/2$ is the density of ordinary energy of the universe which accounts for only about 4.5% of the total energy while the rest, namely 1 − 4.5 = 95.5% is what has been dubbed the missing dark energy. Not only that but we established an analogous situation to a fundamental problem in condensed matter physics and showed that the very same mathematics govern the behaviour of electrons in metals as explained within the theory of gap labelling of Schrödinger operators [8].

From all of the above we have considerable renewed confidence in our proposal made some two decades ago that the universe as a whole can be regarded as huge quasicrystals [37]-[43]. Clearly the proposal is indirectly implied by the work of Penrose [38] as well as a powerful but largely unsung work of a Russian school [41]. The idea was then given new impulse by the work of a leading physicist and cosmologist, P. Steinhardt [43] and it may be possible to explain the origin of the forbidden 5-D symmetry of the found meteorite remnants by the effect of the quasicrystalline geometry of quantum spacetime on its initial quantum formation [36]. In fact all recent astrophysical observations indicate a quasi self-similar universe as exposed in an excellent 2008 paper by R. Murdzek [44], which we give here together with the superb historical account in [6] as recommended reading. We think that future research following the ideas presented here may lead to a possible harnessing of dark energy using some innovative nanotechnological devices.

References

[1] Aoki, H. (Chairman) (2010) Condensed Matter Physics Meets High Energy Physics. *IPMU*, 1*st International Conference*, Tokyo, 8-12 February 2010.

[2] El Naschie, M.S. (1977) The Logic of Interdisciplinary Research. *Chaos, Solitons & Fractals*, **8**, vi-x.

[3] Sachder, S. (2011) Quantum Phase Transition. 2nd Edition, Cambridge University Press, Cambridge.

http://dx.doi.org/10.1017/CBO9780511973765

[4] El Naschie, M.S. (2005) Experimental and Theoretical Arguments for the Number and the Mass of the Higgs Particle. *Chaos, Solitons & Fractals*, **23**, 1091-1098. http://dx.doi.org/10.1016/j.chaos.2004.08.001

[5] French, A. and Kennedy, P., Eds. (1985) Niels Bohr—A Centenary Volume. Harvard University Press, Cambridge-Mass.

[6] Baryshev, Y. and Teerikorpi, P. (2002) Discovery of Cosmic Fractals. World Scientific, Singapore.

[7] El Naschie, M.S. (2004) A Review of E-Infinity and the Mass Spectrum of High Energy Particle Physics. *Chaos, Solitons & Fractals*, **19**, 209-236. http://dx.doi.org/10.1016/S0960-0779(03)00278-9

[8] Bellissard, J. (1992) Gap Labelling Theorems for Schrödinger's Operators. In: Waldschmidt, M., *et al*., Eds., *From Number Theory to Physics*, Springer, Heidelberg, 538-630. http://dx.doi.org/10.1007/978-3-662-02838-4_12

[9] Sze, S. (1981) Modern Physics of Semiconductors. John Wiley & Sons, New York.

[10] El Naschie, M.S. (1998) Fredholm Operator and the Wave-Particle Duality. *Chaos, Solitons & Fractals*, **9**, 975-978. http://dx.doi.org/10.1016/S0960-0779(98)00076-9

[11] El Naschie, M.S. (1998) Penrose Universe and Cantorian Spacetime as a Model for Noncommutative Quantum Geometry. *Chaos, Solitons & Fractals*, **9**, 931-933. http://dx.doi.org/10.1016/S0960-0779(98)00077-0

[12] Landi, G. (1997) An Introduction to Noncommutative Spaces and Their Geometrics. Springer, Berlin.

[13] El Naschie, M.S. (2013) A Resolution of Cosmic Dark Energy via a Quantum Entanglement Relativity Theory. *Journal of Quantum Information Science*, **3**, 23-26. http://dx.doi.org/10.4236/jqis.2013.31006

[14] Corda, C. (2011) Cosmology of Einstein-Vlasov System in a Weak Modification of General Relativity. *Modern Physics A*, **26**, 362-370.

[15] Corda, C. (2008) A Repulsive Force from a Modification of General Relativity. *International Journal of Theoretical Physics*, **47**, 2679-2685. http://dx.doi.org/10.1007/s10773-008-9705-2

[16] Tang, W., Li, Y., Kong, H.Y. and El Naschie, M.S. (2014) Nonlocal Elasticity to Nonlocal Spacetime and Nanoscience. *Bubbfil Nanotechnology*, **1**, 3-12.

[17] El Naschie, M.S. (2014) From Modified Newtonian Gravity to Dark Energy via Quantum Entanglement. *Journal of Applied Mathematics and Physics*, **2**, 803-806.

[18] He, J.H. (2014) A Tutorial Review on Fractal Spacetime and Fractional Calculus. *International Journal of Theoretical Physics*, **53**, 3698-3718. http://dx.doi.org/10.1007/s10773-014-2123-8

[19] Marek-Crnjac, L. and He, J.H. (2013) An Invitation to El Naschie's Theory of Cantorian Space-Time and Dark Energy. *International Journal of Astronomy and Astrophysics*, **3**, 464-471. http://dx.doi.org/10.4236/ijaa.2013.34053

[20] He, J.H. and Marek-Crnjac, L. (2013) The Quintessence of El Naschie's Theory of Fractal Relativity and Dark Energy. *Fractal Spacetime and Noncommutative Geometry in Quantum and High Energy Physics*, **3**, 130-137.

[21] Helal, M.A., Marek-Crnjac, L. and He, J.H. (2013) The Three Page Guide to the Most Important Results of M. S. El Naschie's Research in E-Infinity Quantum Physics and Cosmology. *Open Journal of Microphysics*, **3**, 141-145.

[22] El Naschie, M.S. (2014) Compactified Dimensions as Produced by Quantum Entanglement, the Four Dimensionality of Einstein's Smooth Spacetime and 'tHooft's 4-ε Fractal Spacetime. *American Journal of Astronomy & Astrophysics*, **2**, 34-37.

[23] El Naschie, M.S. (2014) Cosmic Dark Energy Density from Classical Mechanics and Seemingly Redundant Riemannian Finitely Many Tensor Components of Einstein's General Relativity. *World Journal of Mechanics*, **4**, 153-156. http://dx.doi.org/10.4236/wjm.2014.46017

[24] El Naschie, M.S. (2014) From Chern-Simon Holography and Scale Relativity to Dark Energy. *Journal of Applied Mathematics and Physics*, **2**, 634-638.

[25] El Naschie, M.S. (2014) Why E Is Not Equal mc^2. *Journal of Modern Physics*, **5**, 743-750. http://dx.doi.org/10.4236/jmp.2014.59084

[26] Connes, A. (1994) Noncommutatie Geometry. Academic Press, San Diego.

[27] El Naschie, M.S. (2009) The Theory of Cantorian Spacetime and High Energy Particle Physics (An Informal Review). *Chaos, Solitons & Fractals*, **41**, 2635-2646. http://dx.doi.org/10.1016/j.chaos.2008.09.059

[28] Auffray, J.P. (2014) E-Infinity Dualities, Discontinuous Spacetimes, Xonic Quantum Physics and the Decisive Experiment. *Journal of Modern Physics*, **5**, 1427-1436. http://dx.doi.org/10.4236/jmp.2014.515144

[29] Hawking, S.W. and Ellis, G.F.R. (1973) The Large Scale Structure of Spacetime. Cambridge University Press, Cambridge.

[30] Karpenkov, O. (2013) Geometry of Continued Fractions. Springer, Berlin.

http://dx.doi.org/10.1007/978-3-642-39368-6

[31] Jacobsen, L., Ed. (1989) Analytic Theory of Continued Fractions. Lecture Notes No. 1406 in Mathematics. Springer, Berlin.

[32] Khanin, K., Dias, J.L. and Marklof, J. (2007) Multidimensional Continued Fractions, Dynamical Renormalization and KAM Theory. *Communications in Mathematical Physics*, **270**, 197-231. http://dx.doi.org/10.1007/s00220-006-0125-y

[33] El Naschie, M.S. (2013) A Unified Newtonian-Relativistic Quantum Resolution of the Supposedly Missing Dark Energy of the Cosmos and the Constancy of the Speed of Light. *International Journal of Modern Nonlinear Theory and Application*, **2**, 43-54.

[34] El Naschie, M.S. (2013) Nash Embedding of Witten's M-Theory and the Hawking-Hartle Quantum Wave of Dark Energy. *Journal of Modern Physics*, **4**, 1417-1428. http://dx.doi.org/10.4236/jmp.2013.410170

[35] El Naschie, M.S. (2014) On a New Elementary Particle from the Disintegration of the Symplectic 'tHooft-Veltman-Wilson Fractal Spacetime. *World Journal of Nuclear Science and Technology*, **4**, 216-221. http://dx.doi.org/10.4236/wjnst.2014.44027

[36] El Naschie, M.S. and Helal, A. (2013) Dark Energy Explained via the Hawking-Hartle Quantum Wave and the Topology of Cosmic Crystallography. *International Journal of Astronomy and Astrophysics*, **3**, 318-343.

[37] El Naschie, M.S. (2000) Branching Polymers, Knot Theory and Cantorian Spacetime. *Chaos*, *Solitons & Fractals*, **11**, 453-463. http://dx.doi.org/10.1016/S0960-0779(98)00092-7

[38] El Naschie, M.S. (1993) Penrose Tiling, Semi-Conduction and Cantorian l/f^{α} Spectra in Four and Five Dimensions. *Chaos*, *Solitons & Fractals*, **3**, 489-491. http://dx.doi.org/10.1016/0960-0779(93)90033-W

[39] El Naschie, M.S. (1994) Forbidden Symmetries, Cantor Sets and Hypothetical Graphite. *Chaos*, *Solitons & Fractals*, **4**, 2269-2272. http://dx.doi.org/10.1016/0960-0779(94)90046-9

[40] Iovane, G., Laserra, E. and Tortoriello, F.S. (2004) Stochastic Self-Similar and Fractal Universe. *Chaos*, *Solitons & Fractals*, **20**, 415-426. http://dx.doi.org/10.1016/j.chaos.2003.08.004

[41] Ivanenko, D.D. and Gailuin, R.V. (1995) Quasicrystal Model of the Universe. (TpXVIIMexΔyHap.ceMnHapano ϕn3.Bblaconx) (In Russian)

[42] Iovane, G. (2005) Mohamed El Naschie's E-Infinity Cantorian Spacetime and Its Consequence in Cosmology. *Chaos*, *Solitons & Fractals*, **25**, 775-779. http://dx.doi.org/10.1016/j.chaos.2005.02.024

[43] Wolchover, N. (2014) Quasicrystal Meteorite Exposes Novel Processes in Early Solar System. *Scientific American*, 18 June, and *Quanta Magazine.* www.quantamagazine.org/20140613-quasicrystal-meteorite-posses-age-old-questions/

[44] Murdzek, R. (2008) Hierarchical Cantor Set in the Large Scale Structure with Torus Geometry. *Chaos*, *Solitons & Fractals*, **38**, 1269-1273. http://dx.doi.org/10.1016/j.chaos.2007.01.150